

Supplemental Results

Title: Balance of macrophage activation by a complex coacervate-based adhesive drug carrier facilitates diabetic wound healing

Authors: Ching-Shuen Wang¹, Shen-Dean Luo², Shi-hai Jia³, Chen-Han Wilfred Wu⁴, Shwu-Fen Chang⁵, Sheng-Wei Feng¹, Chieh-Hsiang Yang⁶, Jiann-Her Lin⁷ and Yinshen Wee^{8*}

1 School of Dentistry, College of Oral Medicine, Taipei Medical University, Taipei 110, Taiwan.

2 Department of Otolaryngology, Kaohsiung Chang Gung Memorial Hospital and Chang Gung University College of Medicine, Kaohsiung , Taiwan.

3 Department of Neurobiology University of Utah, Salt Lake City, UT 84112, USA.

4 Department of Genetics and Genome Sciences, School of Medicine, Case Western University, Cleveland OH 44106, USA.

5 Graduate Institute of Medical Sciences, College of Medicine, Taipei Medical University, Taipei 110, Taiwan.

6 Department of Oncological Sciences, University of Utah, Salt Lake City, UT 84112, USA.

7 Department of Neurosurgery, Taipei Medical University Hospital, Taipei 110301, Taiwan.

8 Department of Pathology, University of Utah, Salt Lake City, UT 84112, USA.

*Correspondence: yin.wee@hsc.utah.edu; Tel.: +01-801-213-4217.

Keywords: complex coacervates, oligochitosan, phytic acid, sustained release, diabetic wound healing, M2 macrophage polarization, db/db diabetic model.

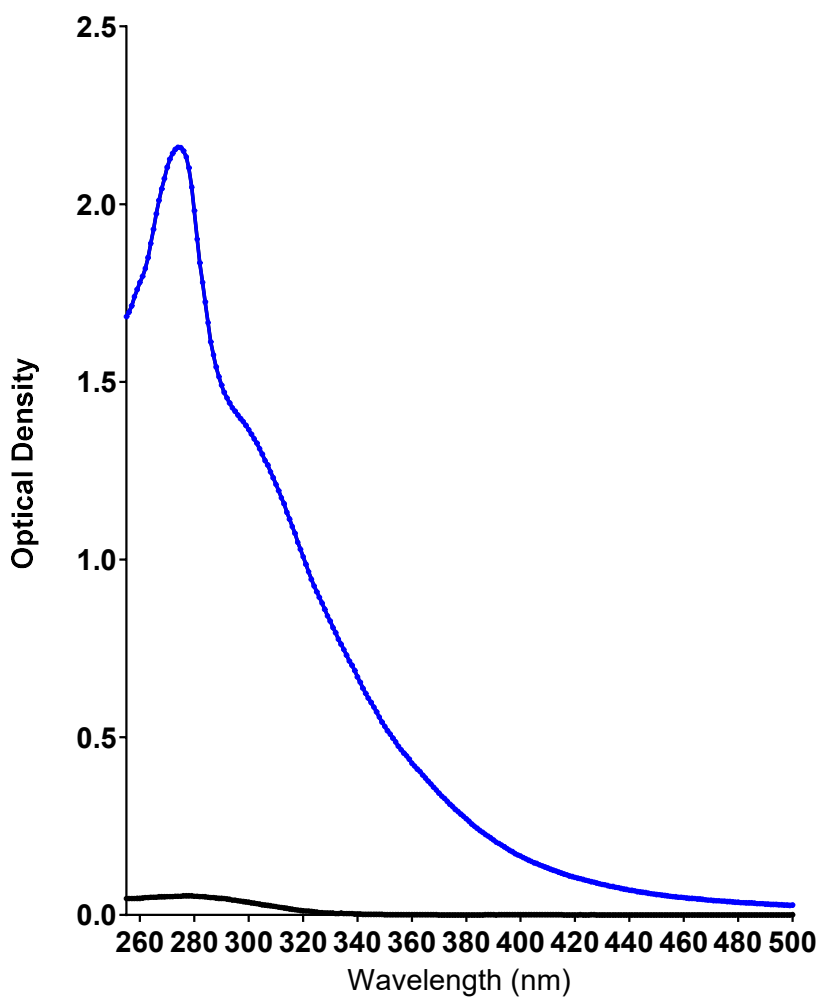


Fig. S1. UV spectrum of Och and IP6. The UV–Vis spectra (240–500nm) of Och (blue line) and IP6 (black line) solution.

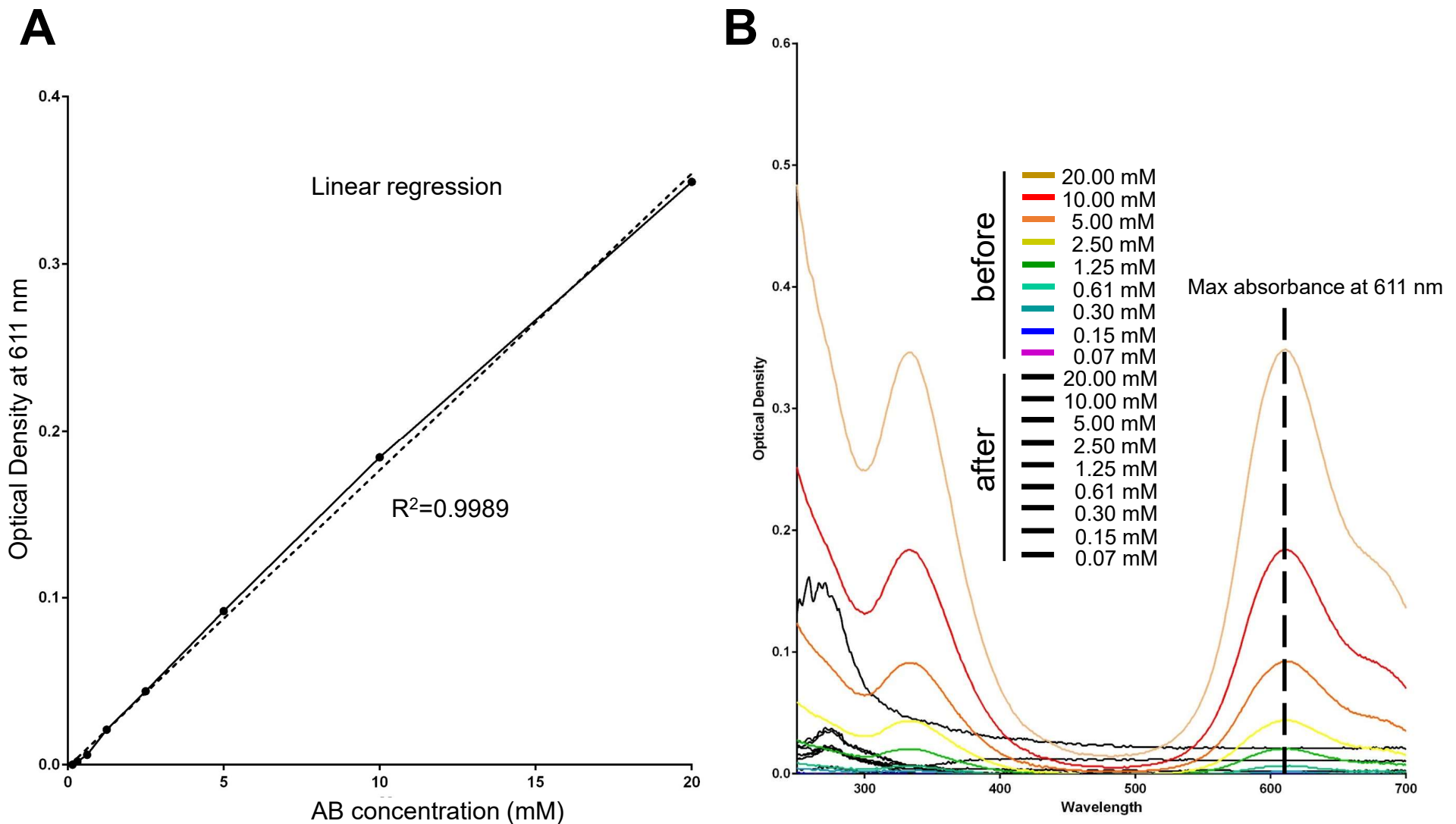


Fig. S2. The encapsulation capacity of Alcian Blue (AB) into the ADC system. (A) UV absorbance intensity as a function of AB concentration in solution. (B) The UV–Vis spectra of AB solution before and after the loading into ADC system.

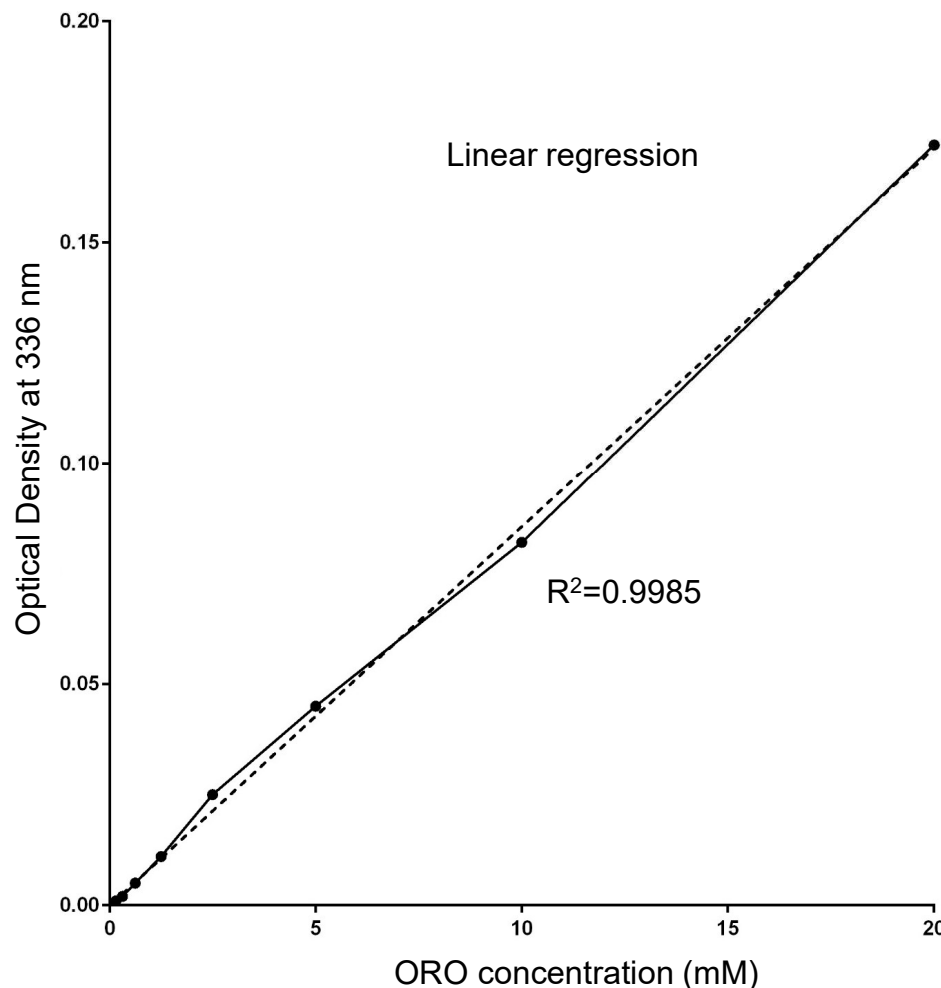
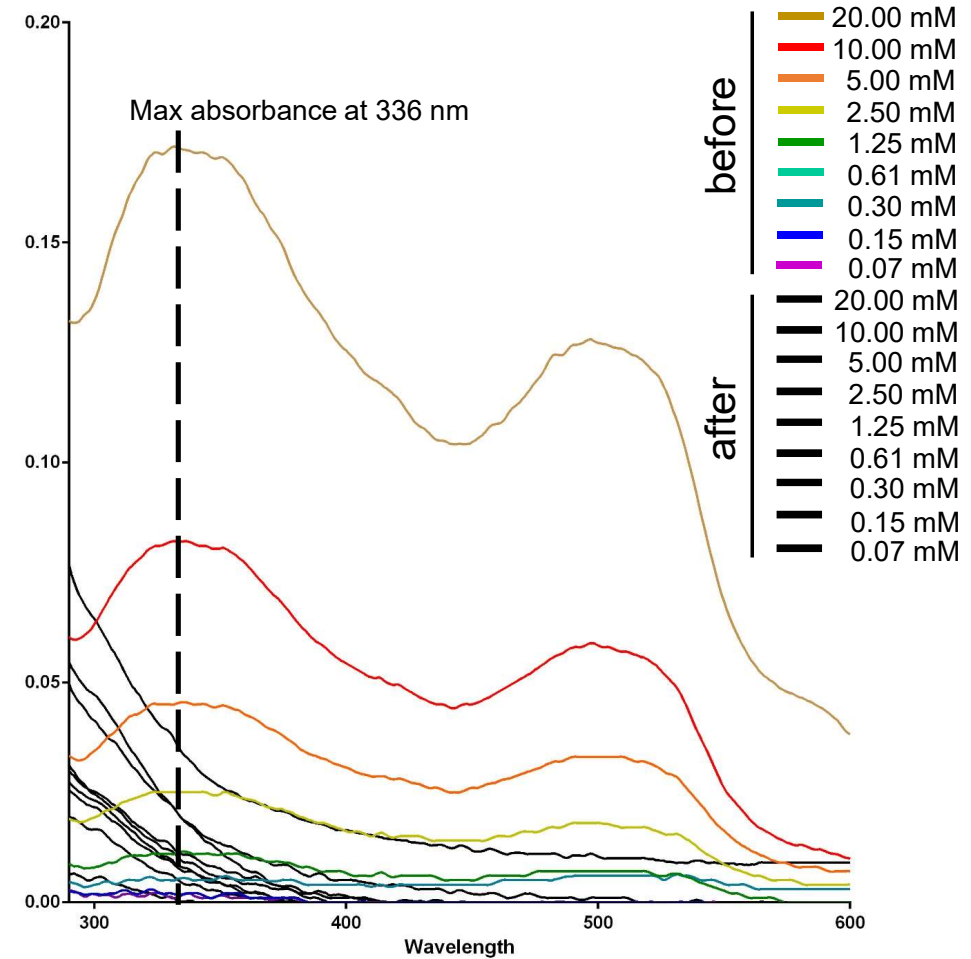
A**B**

Fig. S3. The encapsulation capacity of Oil Red O (ORO) into the ADC system. (A) UV absorbance intensity as a function of ORO concentration in solution. **(B)** The UV–Vis spectra of ORO solution before and after the loading into ADC system.

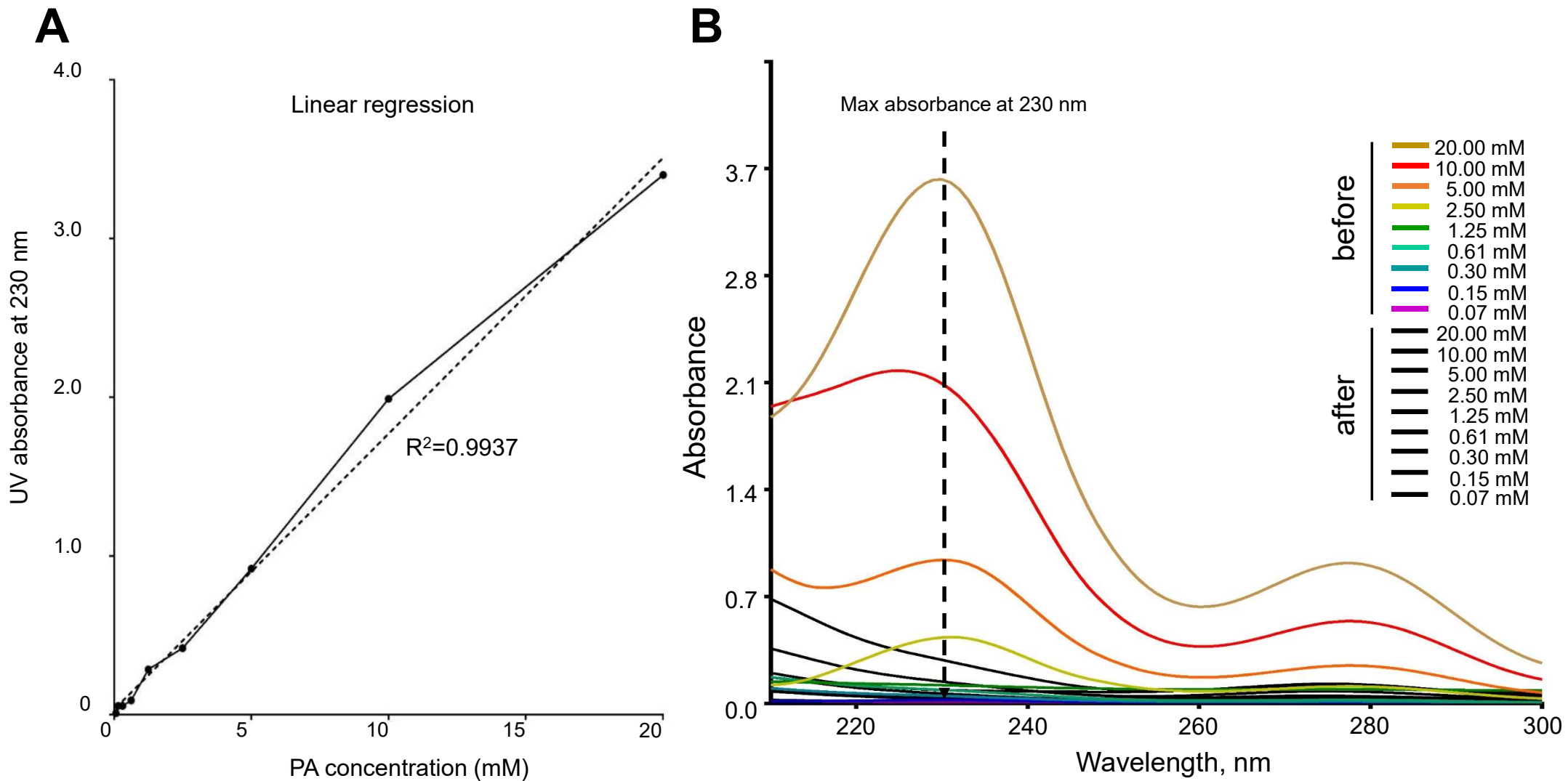


Fig. S4. The encapsulation capacity of proanthocyanidins (PA) into the ADC system. (A) UV absorbance intensity as a function of PA concentration in solution. (B) The UV–Vis spectra of PA solution before and after the loading into ADC system.

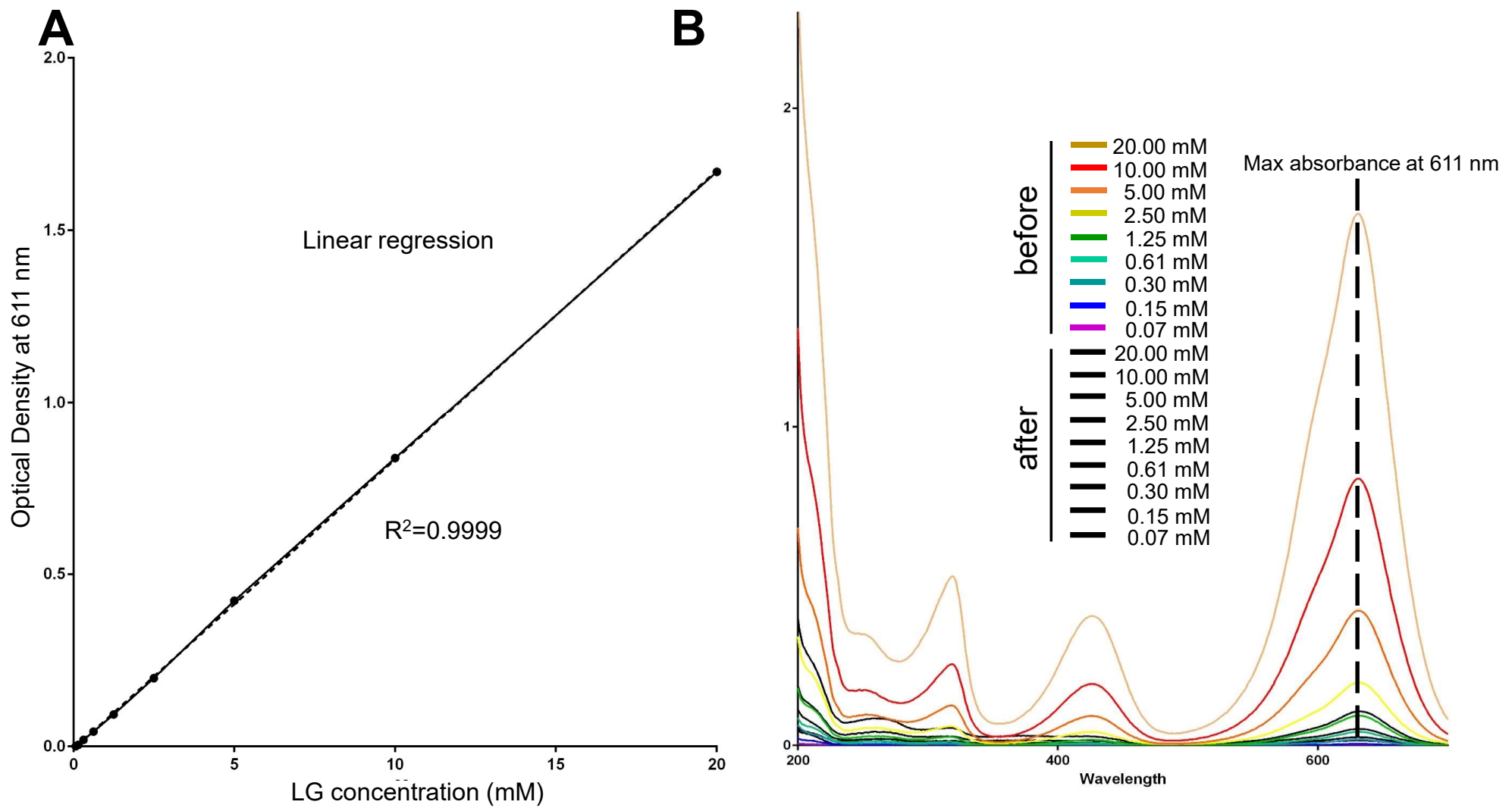


Fig. S5. The encapsulation capacity of light green SF (LG) into the ADC system. (A) UV absorbance intensity as a function of LG concentration in solution. (B) The UV–Vis spectra of LG solution before and after the loading into ADC system.

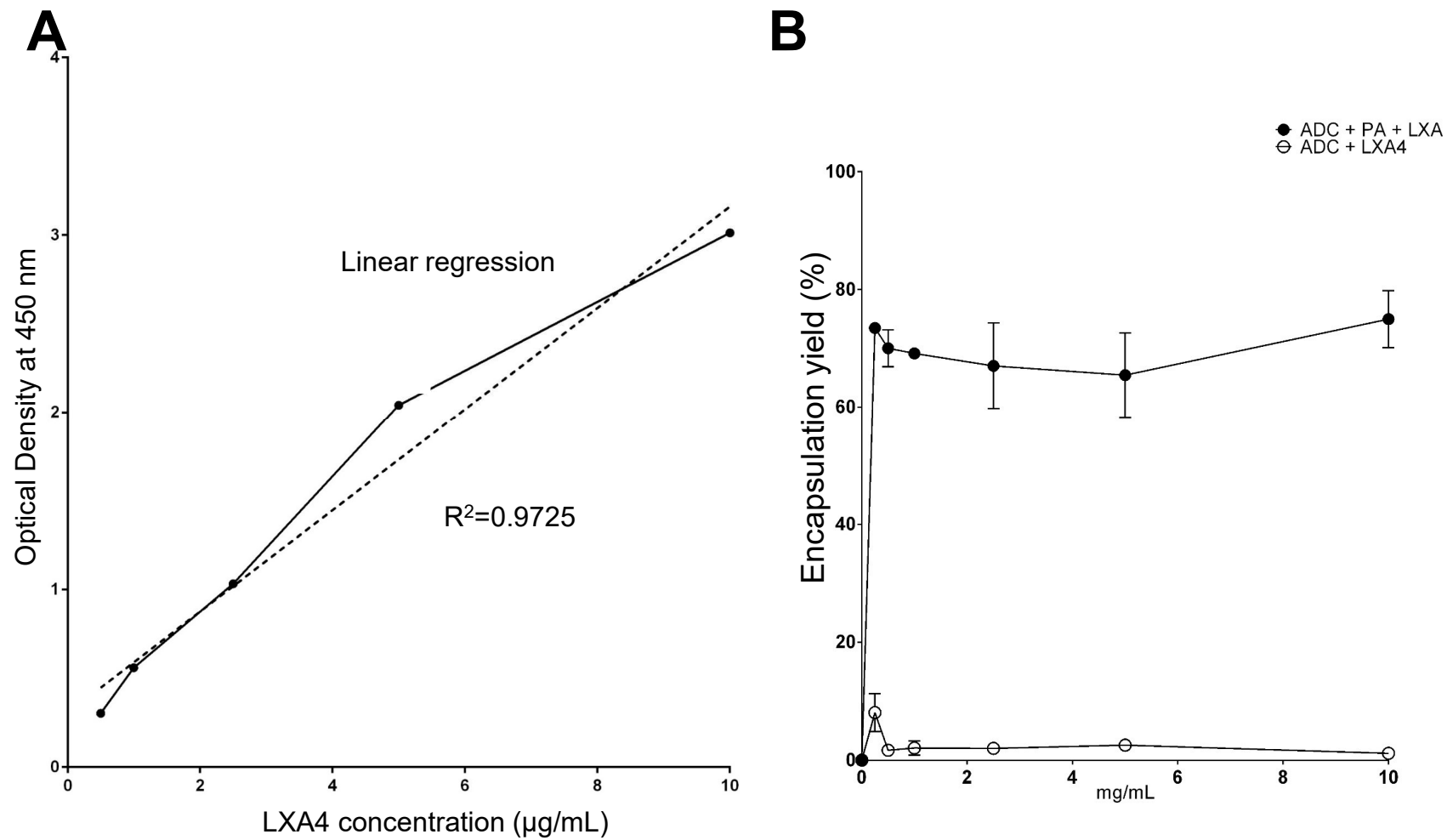


Fig. S6. The encapsulation capacity of lipid mediator lipoxin A4 (LXA4) into the ADC system. (A) UV absorbance intensity as a function of LXA4 concentration in solution. (B) The ELISA result of LXA4 solution before and after the loading into ADC system.

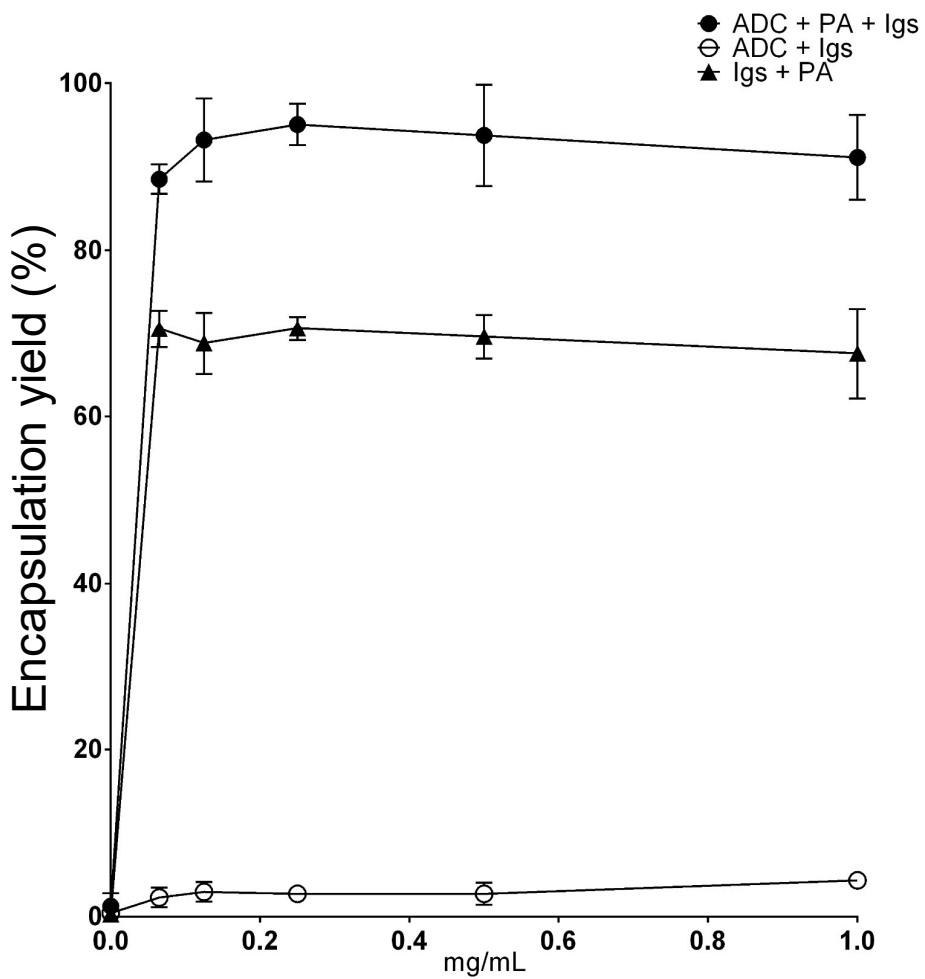


Fig. S7. The encapsulation capacity of fluorescent-labeled immunoglobulin (IgG) into the ADC system. The ELISA result of IgG solution before and after the loading into ADC system.

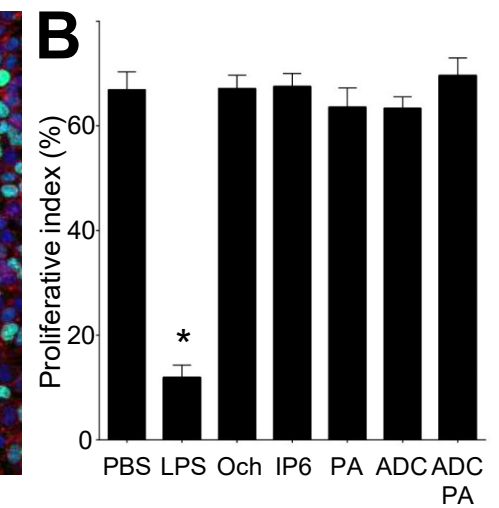
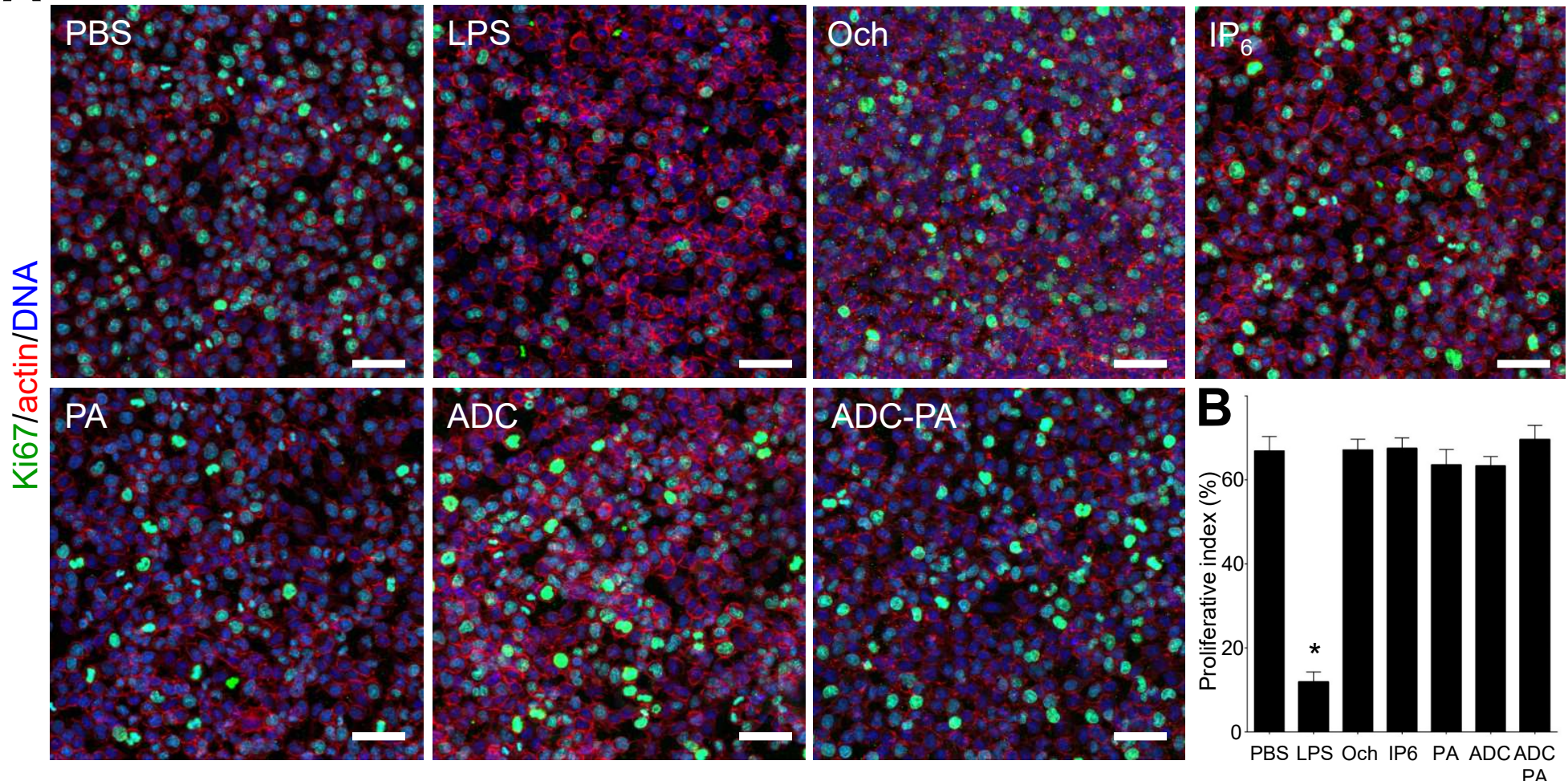
A

Fig. S8. Treatment with ADC or ADC-PA do not affect the proliferation in J774 macrophages. (A) Immunofluorescence staining of the proliferation marker Ki67 in each group: Actin (red), Ki67 (green), and DNA (blue). The results from three independent experiments and representative images are shown. Scale bars = 50 μ m. (B) Statistical analysis of Ki-67-positive cells in each group. The results from three independent experiments are presented as the mean \pm SD. * $p < .05$.

Supplementary Table. 1. Primers used in this study.

Genes	Forward (5'-3')	Reverse (5'-3')	Ccl5	CCACTTCTCTGGTTGG	GTGCCACGTCAAGGAGTAT	Mrc-1	GTGGATTGTTGTGGAGCA	TTGTGGTGAGCTGAAAGGTG
Tnf α	CTGTAGCCCACGTCGTAGC	TTGAGATCCATGCCGTTG	Cox2	CCCCCACAGTCAAAGACACT	CTCATACCCCCACTCAGGAT	mTOR	TATTCCAACACCCAGAAGC	CATATGCCAAGCACTGCAC
Actin	GTAACAATGCCATGTTCAAT	CTCCATCGGGCCGCTTAG	Nlrp3	ATTACCCGCCGAGAAAGG	CATGAGTGTGGCTAGATCCAAG			
IL1 β	TGTAATGAAAGACGGCACACC	TCTTCTTGGGTATTGCTTGG	15lox	CAG GGA TCG GAG TAC ACG TT	GAT TGT GCC ATC CTT CCA GT			
IL-6	TCCAGTTGCCTCTGGGAC	GTACTCCAGAAGACCAGAGG	Sod3	CATGCAATCTGCAGGGTACAA	AGAACCAAGCCGGTATCTG			
Tgf β	AAGTTGGCATGGTAGCCCTT	GCCCTGGATAACCAACTATTGC	Ccl17	ACCAAGCTCACCAACTTCCTG	TGCTTCTGGGACTTTCTG			
Arg-1	TTGGGTGGATGCTCACACTG	TTGCCCATGCAGATTCCC	Irf-5	CAGGTTGGCTTCCACTTG	ATGGGGACAAACCCATCTTC			
Egr-2	CAGAGATGGAGCGAAGCTA	TTGACCAGATGAACGGAGTG	Pparg	AGTCCTCACAGCTGTTGCCAAGC	GAGCGGGTGAAGACTCATGTC			
inos	ACCAAGTATAAGGCAAGCA	GCTTCTGGTCGA	Fibcd-1	GGCTCTGTGAACCTTTCCGA	GAAGCTCGTATGCTGCTTG			
Galectin-3	GGAGAGGGAATGATGTTGCCT	TCCTGCTCGTGTACACACA	Creb	ATCAGTTATCCAGTCTCCACAAGTCC	GTGATGGCAGGGCTGAAGTC			
Fizz-1	TCCCAGTGAATACTGATGAGA	CCACTCTGGATCTCCAAGA	Cd161	GTGCTGCTATCTCAGGAGACA	AACCCACATAGTTGCTCAGGG			
Ccl22	TGGAGTAGCTCTCACCA	TCTGGACCTAAAATCTGC	Del-1	TGGCGGAATATGTACCGACCT	TCCCACGTGTTACCTGAATCCA			
C/EBPbeta	GGAGACCGAGCACAAGGT	AGCTGCTGAACAAGTTCCG	Tlr2	CTCTTCAGCAAACGCTGTTCT	GGCGTCTCCCTTATTGTATTG			
Dectin-1	GACTTCAGCACTCAAGACATCC	TTGTGTCGCCAAAATGCTAGG	cMyc	CGGACACACAACGTCTGGAA	AGGATGTAGGCGGTGGCTTT			
Sod1	GTGATTGGGATTGCGCAGTA	TGGTTTGAGGGTAGCAGATGAGT	Irf-4	GCCCAACAAGCTAGAAAG	TCTCTGAGGGTCTGGAAACT			
Stat4	TTGAAGCAGAATTGTTGCCA	CTTCCTATGGAATCCGGC	Fpr2	CTTTGGCTGGTCTGT	TTCCCTAGCCAGGCTCACAGT			
Stat6	CTGGGGTGGTTCTCTTG	TGCCCCGGTCTCACCTAACTA	Stat1	CTGAATTTCCCTCTGGG	TCCCGTACAGATGTCCATGAT			
5lox	CCCCGAGATATCCAGTTGA	CCTGCCAGTGGTCTTGACT	Ym1	GGGCATACCTTATCCTGAG	CCACTGAAGTCATCCATGTC			

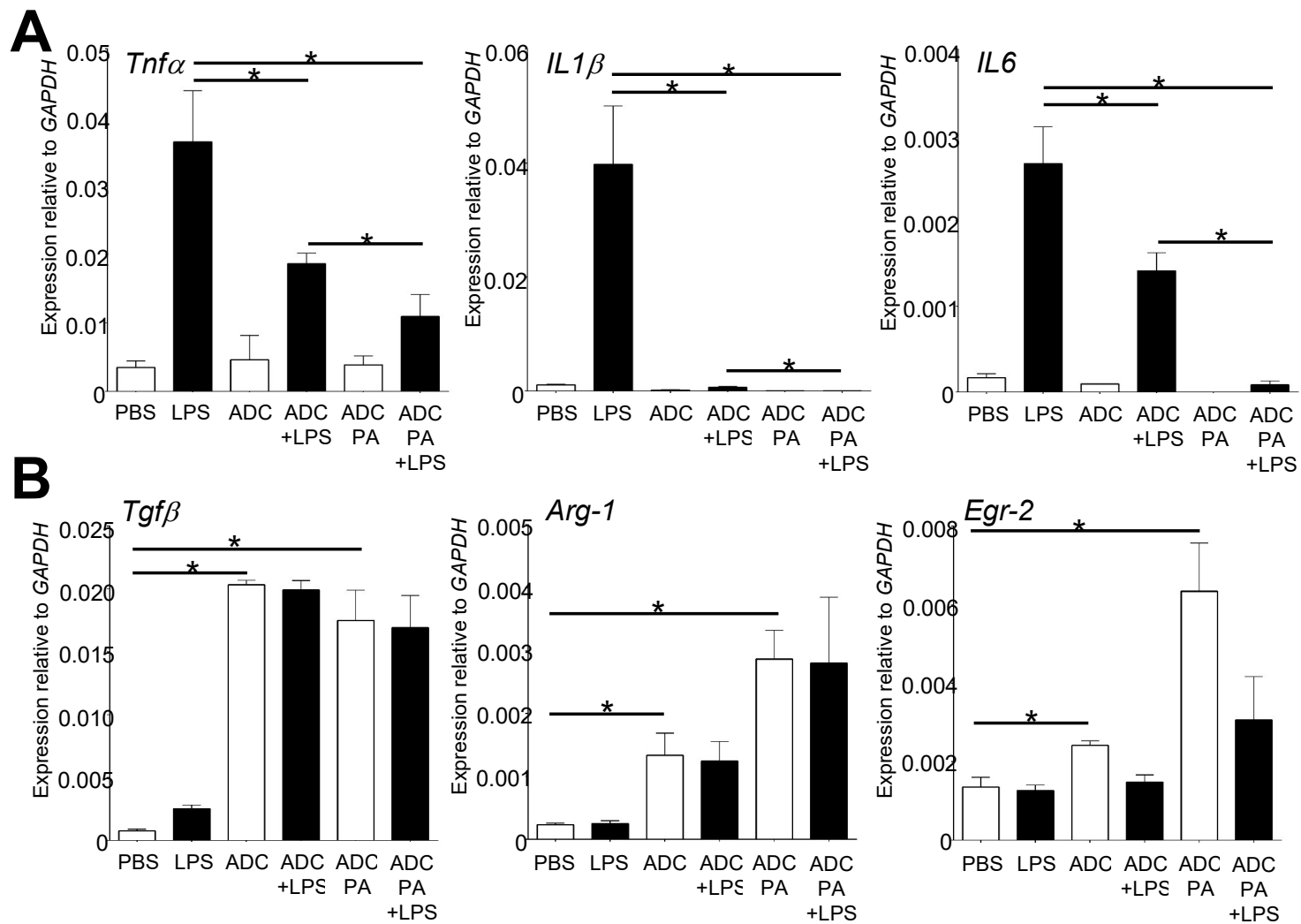


Fig. S9. Treatment with IP6 alters LPS-mediated gene expression in J774 macrophages.
qPCR analysis of (A) pro-inflammatory cytokines and (B) anti-inflammatory cytokines in BMDMs treated with or without ADC or ADC-PA in the presence of LPS stimulation for 24 hr. The results from three independent experiments are presented as the mean \pm SD. * $p < .05$.

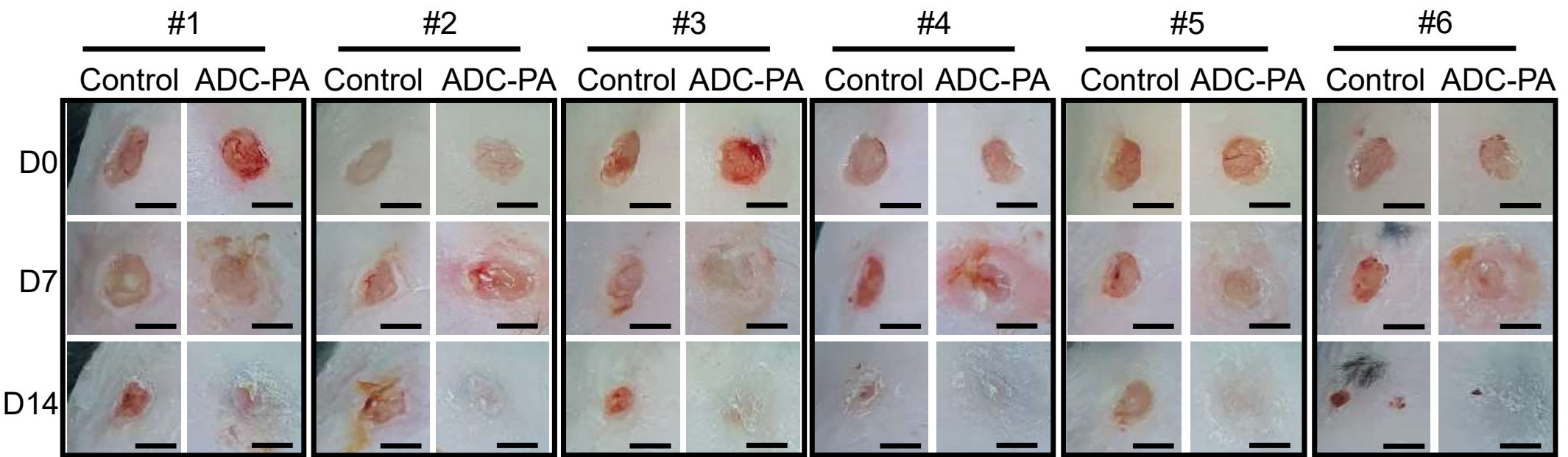


Fig. S10. Healing effects of AC-PA on full-thickness wounds in diabetic db/db mice. Images of wounds from each group over 14-day period post-wounding. Nexcare liquid bandage solution was used as control. Scale bar = 5 mm.

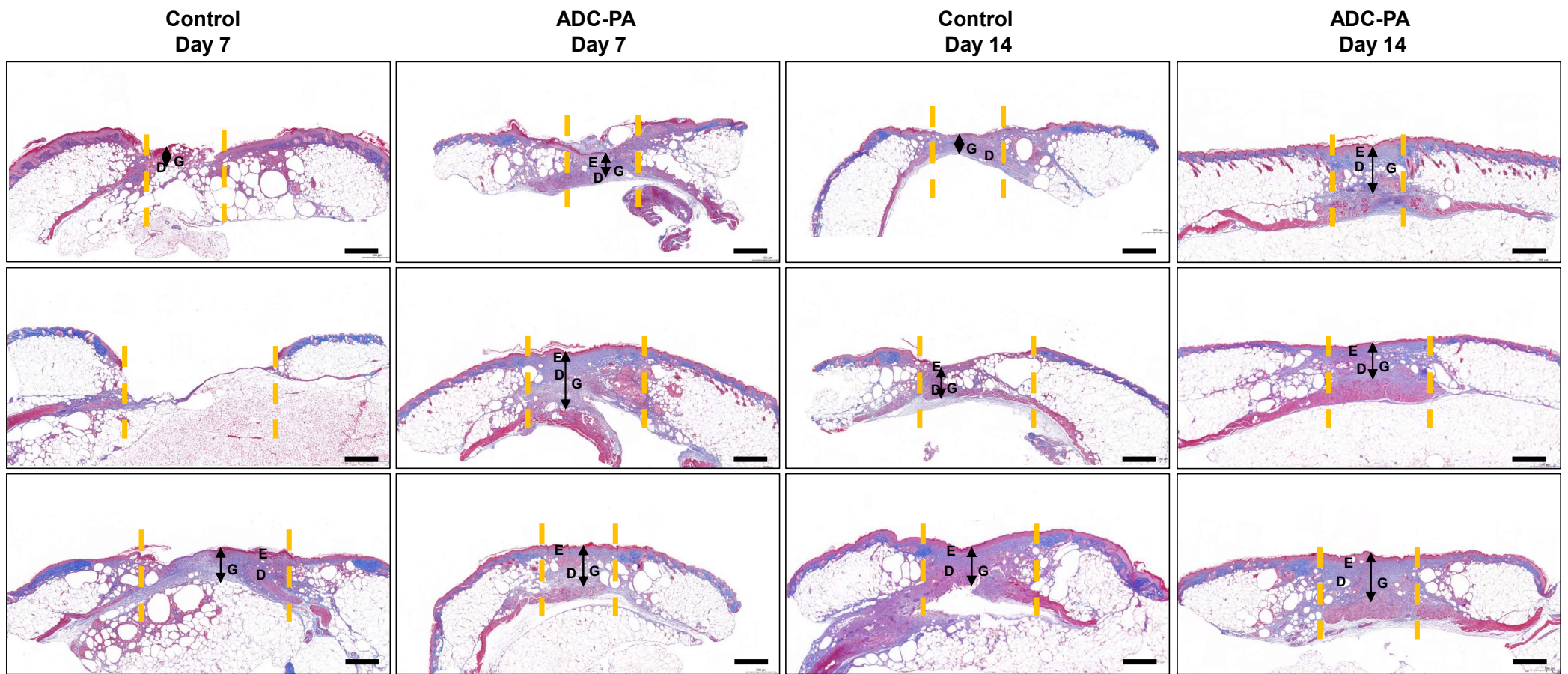


Fig. S11. Healing effects of AC-PA on full-thickness wounds in diabetic db/db mice. Masson's trichrome-stained skin tissue sections on day 7 and 14. Scale bar = 1 mm. Orange dash lines indicate the wound site. Yellow dash lines distinguish the border between epidermis and dermis. Abbreviations: E, epidermis; D, dermis; G, granulation area.

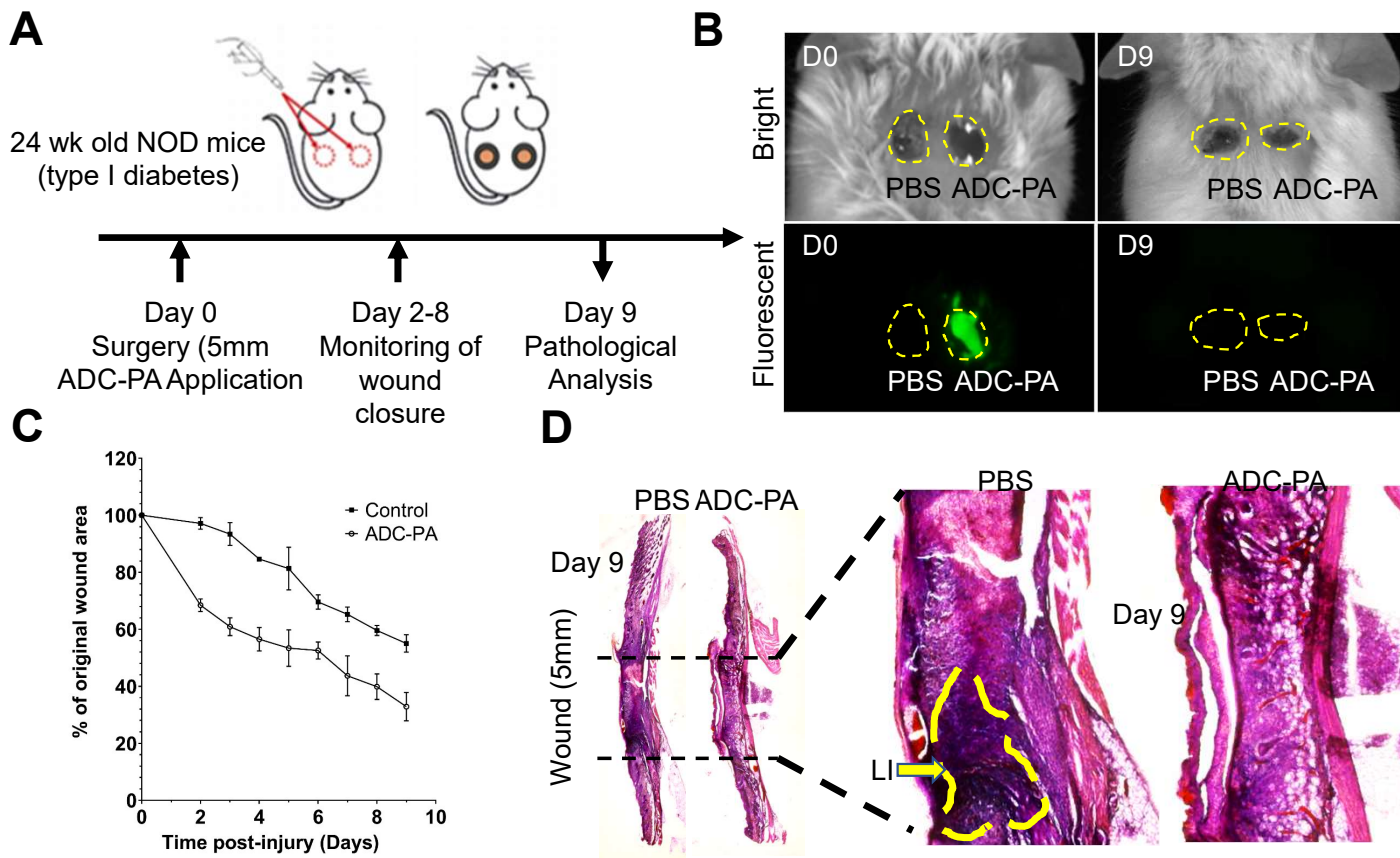


Fig. S12. ADC promotes skin wound healing in NOD mice. Twenty-four-week-old, male NOD mice were used as a model of wound healing. Briefly, full-skin-thickness excisional wounds (5 mm) were created on the dorsum of each mouse using a biopsy punch. (A) Wound conditions on days 0 and 9. ADC is depicted in green due to its autofluorescence. BF, bright-field. (B) Skin wound-closure rate in each group. Wound closure rate was measured daily and calculated based on wound area relative to the original size (D0). (C) Images of longitudinal sections of skin obtained from mice in each group and stained with hematoxylin and eosin (magnification, 4 \times). (D) Magnified images (20 \times magnification) of the areas outlined in black in (C). Yellow circle indicates the area of lymphocytic infiltration. LI lymphocytic infiltration.

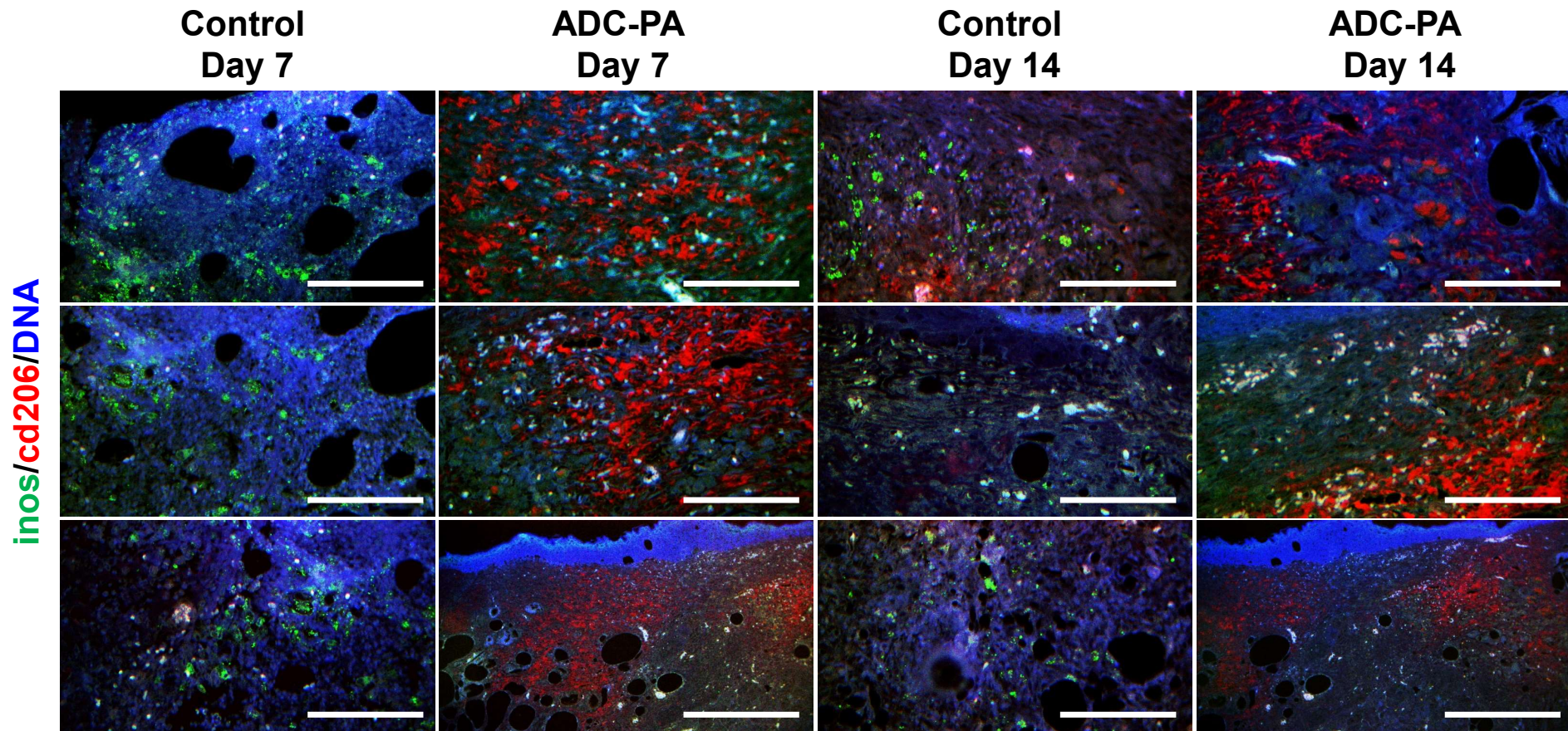


Fig. S13. Significant macrophage polarization from M1- to M2 subtype occurs in ADC-PA treated group.
Fluorescence micrographs showed wounded skin immunostained with M1 marker iNOS (green) and M2 marker CD206 (red) at day 7 and 14. Scale bar = 200 μ m. Abbreviations: iNOS, inducible nitric oxide synthase.